BNL-52645
FORMAL REPORT

GENERATION, TRANSPORT AND DEPOSITION OF TUNGSTEN-OXIDE AEROSOLS AT 1000°C IN FLOWING AIR-STEAM MIXTURES

by

G.A. Greene and C.C. Finfrock
Brookhaven National Laboratory
Upton, New York 11973-5000

October 2001

ENERGY SCIENCES AND TECHNOLOGY DEPARTMENT

Brookhaven National Laboratory
Brookhaven Science Associates
Upton, Long Island, New York 11973-5000

Under Contract No. DE-AC02-98CH10886 with the
UNITED STATES DEPARTMENT OF ENERGY

BNL-52645
FORMAL REPORT

GENERATION, TRANSPORT AND DEPOSITION OF TUNGSTEN-OXIDE AEROSOLS AT 1000°C IN FLOWING AIR-STEAM MIXTURES

by

G.A. Greene and C.C. Finfrock
Brookhaven National Laboratory
Upton, New York 11973-5000

October 2001

ENERGY SCIENCES AND TECHNOLOGY DEPARTMENT

Brookhaven National Laboratory
Brookhaven Science Associates
Upton, Long Island, New York 11973-5000

Under Contract No. DE-AC02-98CH10886 with the
UNITED STATES DEPARTMENT OF ENERGY

DISCLAIMER

Printed in the United States of America
Available from
National Technical Information Service
U.S. Department of Commerce
5285 Port Royal Road
Springfield, VA 22161

ABSTRACT

Experiments were conducted to measure the rates of oxidation and vaporization of pure tungsten rods in flowing air, steam and air-steam mixtures in laminar flow. Also measured were the downstream transport of tungsten-oxide condensation aerosols and their region of deposition, including plateout in the superheated flow tube, rainout in the condenser and ambient discharge which was collected on an array of sub-micron aerosol filters. The nominal conditions of the tests, with the exception of the first two tests, were tungsten temperatures of 1000 °C, gas mixture temperatures of 200 °C and wall temperatures of 150 °C to 200 °C.

It was observed that the tungsten oxidation rates were greatest in all air and least in all steam, generally decreasing non-linearly with increasing steam mole fraction. The tungsten oxidation rates in all air were more than five times greater than the tungsten oxidation rates in all steam. The tungsten vaporization rate was zero in all air and increased with increasing steam mole fraction. The vaporization rate became maximum at a steam mole fraction of 0.85 and decreased thereafter as the steam mole fraction was increased to unity.

The tungsten-oxide was transported downstream as condensation aerosols, initially flowing upwards from the tungsten rod through an 18-inch long, one-inch diameter quartz tube, around a 3.5-inch radius, 90° bend and laterally through a 24-inch horizontal run. The entire length of the quartz glass flow path was heated by electrical resistance clamshell heaters whose temperatures were individually controlled and measured. The tungsten-oxide plateout in the quartz tube was collected, nearly all of which was deposited at the end of the heated zone near the entrance to the condenser which was cold. The tungsten-oxide which rained out in the condenser as the steam condensed was collected with the condensate and weighed after being dried. The aerosol smoke which escaped the condenser was collected on the sub-micron filter assemblies.

There was no aerosol generation for the case of all air, so the plateout, condensate and smoke were all zero. For the case of all steam, there was very little plateout in the superheated regions (several percent) and the rest of the aerosol was collected in the condensate from the condenser. There was no smoke discharge into the filters. For the experiments with intermediate air-steam fractions, there was some aerosol plateout, considerable aerosol in the condensate and aerosol smoke discharged from the condenser with the escaping air.

TABLE OF CONTENTS

LIST OF TABLES

LIST OF FIGURES

NOMENCLATURE

d, d_h	diameter, hydraulic diameter
DF	WO_3 aerosol decontamination factor, see Fig. 10
ΔH	heat of vaporization (cal/g-mol)
$\dot{m}''$	mass flux (g/cm^2·s)
$\dot{m}''_{W,steam}$	W vaporization rate in 100% steam (g/cm^2·s), see Eq. (1)
$\dot{m}''_{WO3,aerosol}$	WO_3 aerosol discharge rate (g/cm^2·s)
$\dot{m}^*_{WO3,aerosol}$	normalized WO_3 aerosol discharge rate = $0.793*(\dot{m}''_{WO3,aerosol}/\dot{m}''_{W,steam})$, see Fig. 11
$\dot{m}''_{W,vap}$	W vaporization rate (g/cm^2·s)
$\dot{m}^*_{W,vap}$	normalized W-vaporization rate = $\dot{m}''_{W,vap} / \dot{m}''_{W,steam}$, see Fig. 8
$\dot{m}''_{W,ox}$	W oxidation rate (g/cm^2·s)
$\dot{m}^*_{W,ox}$	normalized W-oxidation rate = $\dot{m}''_{W,ox} / \dot{m}''_{W,steam}$, see Fig. 6
M_{steam}	steam flow rate (mole/min)
M_{air}	air flow rate (mole/min)
R	universal gas constant (1.987 cal/g-mol·K)
Re	annulus Reynolds number = $(U_{gas}\cdot d_h/\nu_{gas})$
RF	radio frequency
T_W	tungsten temperature
T_{wall}	wall temperature
T_{gas}	gas temperature
U_{gas}	average gas-mixture velocity
W, WO_3	tungsten, tungsten-oxide
ν_{gas}	gas-mixture kinematic viscosity

1. INTRODUCTION

Consideration of overheating accidents for tungsten spallation target assemblies in proton accelerator facilities, such as the APT target as well as other tungsten spallation targets, have shown that radiological releases would be dominated by aerosols generated by the vaporization of tungsten from the target [1-4]. The remainder of the radiological source term would be comprised of volatile and noble gas spallation products and a fraction of the non-volatile spallation products in both the tungsten and the coolant. No reduction in the radiological source term due to aerosol plateout as a result of natural processes was considered in APT accident analyses due to a lack of data to form a basis for such a reduction [5].

Tungsten can be mobilized by vaporization reactions with steam at rates which are quite rapid at temperatures above 1200°C. In order to mitigate the radiological source term for the APT target, the APT baseline target design was modified to clad the tungsten in Inconel 718 to prevent contact of hot tungsten with steam, thus preventing vaporization. Experiments have shown that this clad can survive to 1250°C, a temperature which bounds the thermal conditions for most target accidents [6]. In order to satisfy this thermal limit for the clad performance, other systems have been classified as safety class or safety significant at the expense of large capital investments in facilities and safety systems. However, these results have broader relevance than to just APT because of the current interest in and use of tungsten in other accelerator spallation targets systems under consideration. If natural mechanisms and design features could demonstrate a significant aerosol retention capability for tungsten aerosols under accident conditions, the safety class and safety significant classifications of some systems could be relaxed, resulting in substantial financial savings for future facilities.

2. BACKGROUND

Experiments have been previously conducted with 1/8-inch diameter cylindrical tungsten rods to measure the rate of vaporization of tungsten in flowing steam for the radiological source term for the APT target [7]. The tungsten rods were heated by RF induction heating and steam was supplied to the rods at atmospheric pressure and 140°C from a low pressure boiler. The weight losses from the rods were measured at the different temperatures and, from these data, the rates of vaporization per unit area were correlated to the sample temperatures. The tungsten vaporization rate model which resulted from correlating the experimental data is shown below,

$$\dot{m}''_{W,steam}\ (g/cm^2 \cdot s) = 2611\ \exp[-48900/RT] \qquad (1)$$

where R = 1.987 cal/gm-mol K. This correlation is also shown in graphical form in Fig. 1. The tungsten aerosols that were generated by vaporization were directed through a condenser downstream of the RF test section for collection. There was a short vertical run of heated glass after the test section, followed by a 135° bend downwards, whereupon the aerosol-laden steam entered a glass condenser tube which was cooled by tap water. Some of the tungsten-oxide aerosol deposited on the outside of the 135° bend by impaction; the remainder of the aerosol stream was retained in the condensate as the steam condensed, resulting in 100% aerosol retention with little effort. In spite of these encouraging observations, there was little quantitative data to model the aerosol retention (deposition), therefore aerosol retention was not considered for source term reduction in the APT safety analyses, even though condensation of

the steam carrier gas had been shown to be effective in removing 100% of the aerosol in a flow distance of less than 30 cm.

The circumstances of tungsten vaporization are entirely dependent upon the presence of steam or water vapor in contact with hot tungsten to support the vaporization reactions. It follows that transport of the aerosols is subsequently influenced by the steam as it flows through the remainder of the system. In narrow channels with bends and stagnant volumes, much of the aerosol could be removed by deposition even if the steam were superheated, as occurred in the experiments just discussed [7]. As the steam flows through cold structures such as shielding blocks or coolant pipes, the steam would condense on cold surfaces and trap the aerosols in the condensate. In the tungsten-steam experiments previously reported, 100% aerosol retention was achieved by condensing the steam. If the carrier gas were air, the hot tungsten would oxidize but the hydration of the WO_3 to tungstic acid vapor ($WO_3 \cdot H_2O$ or H_2WO_4) would not occur. As a result, there would be negligible aerosol production. The carrier gas, however, would most likely be a mixture of air and steam in an actual accident; the air-steam mixture might support a lesser rate of tungsten vaporization than the case of all steam, and condensation of the steam should remove much of the aerosols from the gas stream, but probably not all. Both effects were measured in the experiments which are described and discussed below.

3. DESCRIPTION OF TEST FACILITY AND PROCEDURES

In order to quantify these effects, a small-scale experiment was conducted to examine tungsten aerosol formation by vaporization of tungsten in air-steam mixtures as well as aerosol removal by deposition and condensation in downstream flow paths. Rods of pure tungsten at

high temperatures were exposed to varying air-steam mixtures to evaluate the effects of the steam mole fraction on the rate of vaporization of tungsten. The air-steam mixtures were chosen to cover a range of conditions which could be expected in APT target accidents. The tungsten vaporization rates for such gas mixtures are compared to the results for 100% steam as given in Eq. (1). The principal flow paths were simulated downstream of the exit of the tungsten test section by vertical and lateral pipe runs with various inlet and boundary conditions, as well as geometrical configurations to represent flow paths through blanket modules and shielding. The results of these tests will be examined to evaluate tungsten vaporization and aerosol formation in air-steam mixtures instead of all steam to see if any reductions in the tungsten vaporization can be realized. The results will also be examined to evaluate the magnitude of the effects of aerosol retention as the aerosol-laden air-steam mixtures flow through cold structures to see if impaction and condensation result in significant aerosol retention in such structures and if significant reductions in the radiological source terms can be realized by accounting for such phenomena. Descriptions of the test apparatus, calibrations and procedures are given below. Schematic and photographic views of the instrumentation and hardware are given in Figs. 2-4.

3.1 Lepel RF Power Supply

The tungsten rods were heated to their intended temperatures by RF induction heating. The induction heating generator, Lepel Model T-10-3-KC-TL, was specifically designed for such industrial heating applications. The electrical system consisted of three elements: a control system, a high voltage DC supply to convert line voltage to high voltage DC, and the modified Hartley oscillator to convert the high voltage DC power to RF output power. The tapped tank

coil and variable grid coil provided flexibility for matching a wide variety of workpieces and load coils to the generator output. The specifications of the system provide a maximum of 10 kW RF power output in the 200-450 kHz output frequency range. The output was regulated to provide continuous control from zero power to 100% power with very short response time. Control could be manual or automatic. The system was configured for manual control for the aerosol tests.

3.2 Tungsten Temperature Measurement

The tungsten aerosol source was generated by reactive vaporization of a cylindrical tungsten rod by RF induction heating. It was desirable to measure the rate of vaporization of tungsten at known temperatures in various air-steam mixtures as well as the aerosol behavior; therefore it was important to know the tungsten rod temperatures accurately. The tungsten rod temperature was measured by a Pyro Photo II optical pyrometer useful for temperatures from 760°C to above 3000°C. The pyrometer was calibrated to a tungsten ribbon filament strip lamp whose output current characteristics have been certified by commercial calibration to a regulated 12 VDC power supply to NIST Test Certificate No. 844/247425-91. Using the ribbon filament lamp as a calibration standard, the pyrometer output voltage was measured in multiple temperature ranges; the calibration curve for the range 900°C to 1400°C was based on a curve fit to 330 data points with a maximum uncertainty of ±3°C. The output of the pyrometer was measured by the data acquisition and control system and displayed in real time for manual control of the Lepel RF power supply during the experiments.

3.3 Flow Path Heaters

Heat was supplied to the quartz glass aerosol flow channel by a series of modular ceramic heaters. For straight runs of piping, a pair of semi-cylindrical heaters were wired in series and clamped to form a cylindrical shell. Each semi-cylindrical element has a maximum voltage drop of 120 VAC to deliver a heater power of 425 W each. Thus the maximum power output from a pair of semi-cylindrical heaters wired in series was 850 W. For right-angle bend regions, a pair of flat plate heaters were combined in parallel with unheated ceramic board to make a box heater with two open sides. This assembly would mate to the faces of the adjacent cylindrical heaters to complete the corner box with no openings in the heated zone. Each flat plate heater has a maximum voltage drop of 60 VAC to deliver a heater power of 400 W each; thus the maximum power output from a pair of flat plate heaters wired in series is 800 W. The flat plate heaters which use a helically-wound ribbon are rated to 1200°C; the semi-cylindrical heaters which use a helically-wound wire are rated to 1100°C. The modular heater pairs have been sized to accommodate up to two-inch diameter quartz glass in any shape which includes straight runs in increments of six inches and 90° bends with a 3.5-inch radius of curvature.

3.4 Steam Supply

Steam was provided to the system by a Reimers boiler capable of providing steam at up to 70 psig and 14 lbm/hr. The actual requirements of these experiments were more modest and the boiler supply was calibrated using a precision vernier-dialed needle valve for flow control up to 10 g/min. Steam flow can be calibrated by diverting the steam to a bypass condenser and weighing the condensate versus time. The steam flow was found to be reproducible and stable

over long periods of time. The boiler was fitted with an automatic fill system so it did not have to be shut off to be refilled.

3.5 Non-Condensable Gas Supply

In addition to steam, metered and regulated non-condensable gases were supplied to the test section. Argon gas was provided for hot, pre-test setup operations to prevent oxidation and vaporization of the tungsten while adjustments were being made to the system. Air was supplied during testing to mix with the steam and provide the desired air-steam mixture to the heated tungsten rods. All gas supplies were three-way valved in order to direct the gases to bypass paths or to the test section conveniently. The non-condensable gases were supplied from compressed gas cylinders of appropriate quality. Both supplies were regulated to a pre-established working pressure and directed to a bank of MKS mass flow controllers for measurement and control. The MKS Series 100 mass flow controllers were controlled by the data acquisition and control computer with slide bar controls and digital readout of the actual flow rates provided on the computer screen. Control of the steam flow rate (manual control) and the air flow rate (computer control) enabled continuous control of various air-steam mixtures. Although calibrated for nitrogen gas, the mass flow controllers can be readily converted to other gases or gas mixtures by application of a gas correction factor (GCF) through software. The GCF for air is 1.00 and for argon is 1.39. After the air, argon and steam had been metered and controlled, their supply lines were trace heated and temperatures controlled up to the inlet of the gas mixture heater assembly.

3.6 Temperature Measurement and Control

The inlet and boundary temperatures were controlled and measured for precise control of inlet and boundary conditions to the glass test section. At least 12 individual heating circuits were actively and continuously monitored throughout the experiments. The first zone was the inlet gas mixture heater assembly just upstream of the tungsten rod. Measurement and control of temperature here established the inlet gas mixture temperature. The quartz glass aerosol flow path can be configured in such a manner to incorporate 11 individual heater zones, each of which must be measured and controlled as well. Each thermal zone was equipped with two 1/16" type-K ungrounded thermocouples, one for temperature measurement and the other for temperature control. Although the thermocouple junctions were not grounded to their sheaths, the sheath of each thermocouple was bonded to earth ground to eliminate electrical pickup from the heater coils. Measurement thermocouples were routed through a Strawberry Tree (Iotech) Data Shuttle Express module which was equipped with electronic thermal reference by means of a platinum resistor on an isothermal block. Each module can measure up to 16 thermocouples. The module then outputs the 16 channels to the data acquisition and control computer for recording and display. The control thermocouples were routed through two six-channel Omega solid-state temperature controllers which controlled the power to the individual heater zones to establish and control the pre-determined temperatures for each zone. The zonal temperatures were set through the data acquisition and control system by software input much the same as non-condensable flows were set. All thermocouples and gas flow rates were continuously recorded at a prescribed sampling rate. Temperatures could be controlled to a pre-set constant as well as programmed for a desired ramp rate.

3.7 Quartz Glass Test Sections

The aerosol flow path downstream of the RF-heated tungsten rod was made of a one-piece quartz glass test section, one inch in diameter. The one-piece quartz glass was shaped into the prescribed geometry by a glass blower and ground glass joints were mounted on each end for smooth transitions without edges to avoid aerosol scraping at the joints. The upstream end mounted to the discharge of the quartz glass rod holder while the downstream end mounted to the condenser assembly. Straight sections were sized in multiples of six inches to permit seamless installation of the six-inch clamshell heaters without gaps. The 90° bends were created in the glass with a 3.5 inch centerline radius of curvature to accommodate the flat plate box heaters and to provide a snug fit between the opposing clamshell heaters and the open faces of the flat plate box heater without gaps for good insulation. The downstream end of the quartz glass test section was angled downward at 60° from horizontal to prevent condensate from backing up into the heated zone. The quartz glass test sections may be reused after an experiment once the aerosol which plated out has been cleaned.

3.8 Condenser S-Trap and Sub-Micron Aerosol Filter Assembly

Upon execution of the first test, it was observed that aerosol smoke was being discharged from the condenser exit which must be collected and weighed. In order to do this, an S-trap with a bottom drain was installed on the discharge of the condenser to separate the condensate which was dripping downwards out of the condenser from the aerosol smoke which was also being discharged downwards. The S-trap collected the condensate and directed it downwards into a beaker for collection while the aerosols continued to flow out the larger discharge end of the

fixture and were directed upwards at 45° from vertical onto the face of a Millipore sub-micron filter assembly. The filter porosity was 0.45 μm, which was adequate to collect the aerosols with no penetration through the media. The filter holder slipped onto the end of a Luer fitting and was continuously purged by a roughing pump during the experiment. The filter media were carefully and precisely tare-weighed prior to use and stored in a desiccator under vacuum until installed. After use, the filters were desiccated and reweighed until a constant weight was recorded.

3.9 Data Acquisition and Control

The experiments were conducted under the control of a customized data acquisition and control program configured from the parent platform Work Bench, a software product of Strawberry Tree. Control panel display of the test parameters and measurements was provided by selecting one of several computer display screens of the data acquisition and control program on the screen of the data acquisition and control computer. The control panel display enabled the operator to set desired gas flow rates and zonal temperatures by mouse operations on the computer screen, greatly reducing the complexity of manual operations and providing a computer record of all test parameters, settings and other identifying data. The data acquisition and control program controlled all test parameters besides the steam flow rate and RF power, and measured all test parameters besides the steam flow rate. The test parameters were continuously controlled for the duration of an experiment and the data were written to a file for analysis.

3.10 Measurements, Calibrations and Certifications

The tungsten rods which were used in these experiments were procured from Schwarzkopf with materials certification of the composition. Temperatures of the tungsten rods were measured with a laboratory-calibrated optical pyrometer. The output voltage of the pyrometer was measured by a calibrated Keithley nanovoltmeter and temperature was inferred from an Osram Sylvania tungsten ribbon filament strip lamp onto which the pyrometer was focused. The tungsten filament strip lamp has a temperature-current calibration certified by NIST under their Test Certificate No. 844/247425-91. The current of the tungsten ribbon filament strip lamp was inferred by the measurement of voltage drop across a calibrated resistance shunt by the same calibrated Keithley nanovoltmeter. Dimensions such as diameter and length were made with recently laboratory-calibrated calipers and micrometers. Masses up to 120 g were measured by a Sartorius Model BP-125 digital balance with a precision of 0.1 mg. The balance has a precision internal 100 g calibration standard which enables precise calibration from the touch pad upon each use. Steam flow was calibrated using a precision vernier-dialed needle valve to control the boiler output and the timed mass of condensate weighed on the Sartorius balance to provide time-averaged steam flow rate. The steam flow calibration could be checked prior to and during each experiment in the exact same manner as part of pre-test procedures. Flows of non-condensable gases were measured by a bank of laboratory-calibrated mass flow controllers. These calibrations were checked in the laboratory by a soap bubble rise time method using a precision burette and a stop watch, a typical method for such calibrations. Temperatures along the quartz glass test section were measured with type-K ungrounded thermocouples. For convenience, the thermocouples were purchased with special-limits-of-error

wire, conforming to ANSI MC 96.1, with a certified temperature measurement uncertainty of 1.1 °C or 0.4%, whichever is greater, over the temperature range of 0 °C to 1250 °C.

3.11 Test Procedures

In preparation for an experiment, a tungsten rod was selected from stock and characterized. These measurements were recorded on hard copy and input to the computer record of the experiment. The clamshell heaters were configured in the appropriate geometry for the specific quartz glass test section to be used. The rod was installed and aligned in the apparatus and the quartz glass test section was positioned on the discharge of the gas mixture heater and into the clamshell heaters which had been opened. Once final adjustments had been made to correctly position all components, the clamshell heaters were clamped shut, the flat plate box heaters were positioned at each 90° bend, and the electrical connections to the heaters were established. A condenser assembly was then mounted to the discharge joint of the quartz glass test section and water flow was established in the condenser annulus. All electrical connections to the heaters were tested, thermocouple installations were verified, and heated argon flow established through the assembly for inert pre-test setup. The boiler was energized and the steam flow rate was verified by condensate collection through a separate condenser.

Once the entire assembly had been configured and flow rates had been verified, the heaters were energized to their desired set point temperatures, the RF was energized to the desired tungsten rod temperature, and the system was monitored until the prescribed steady state conditions were achieved. The system would soak at steady state to verify that set points were being maintained and stability insured. Once these criteria had been satisfied, the desired air and

steam mixture was manually valved in and tare-weighed beakers were rotated in to collect the tungsten-oxide in the condensate. All set-point test parameters were monitored, controlled and recorded by the data acquisition and control system. At the end of the prescribed time, the air-steam mixture was valved out and argon was valved in for the cooldown phase.

Once cold, the quartz glass test section was removed from the heater assembly and post-test operations commenced. The condensate beakers were gently dried, desiccated and weighed. The tungsten rod was weighed and dimensioned. If necessary, the quartz glass test section could be carefully sectioned so as not to disturb the aerosol on the interior surfaces. Each section could be weighed, cleaned and desiccated, and reweighed to determine the mass of tungsten-oxide deposited. In practice, this turned out not to be necessary.

4. DISCUSSION OF TEST RESULTS

Experiments were conducted to measure the rates of oxidation and vaporization of pure tungsten rods in flowing air, steam and air-steam mixtures. The test parameters for these experiments are listed in Table 1. The composition of the tungsten rods was certified to be 99.96% pure. Also measured were the downstream transport of tungsten-oxide condensation aerosols and their region of collection, including plateout in the heated flow tube, rainout in the condenser and ambient discharge which was collected on an array of sub-micron aerosol filters. The gas flow rates in the experiments were low enough to be in laminar flow but adequate to insure that the supply rates of air and steam in the experiments never deprived the tungsten rod of oxidant. In order to characterize the fluid dynamics of the air and steam mixture in the annulus, the Reynolds number for the gas-mixture is defined as follows,

$$Re = U_{gas} \cdot d_h / \nu_{gas} \quad (2)$$

where U_{gas} is the average velocity of the gas mixture in the annulus surrounding the tungsten rod, d_h is the hydraulic diameter of the annulus formed between the 0.3 mm diameter tungsten rod and the 2.18 cm diameter quartz glass retort, and ν_{gas} is the kinematic viscosity of the gas mixture. Reynolds numbers for the annulus varied from 60 to 180, verifying that the flows were well into the laminar flow regime. In addition, the maximum Reynolds numbers along the surfaces of the rods (external flow Reynolds number) were in the range 300 to 900, similarly in the laminar flow regime. All the tests with the exception of the first two had tungsten temperatures of 1000°C (a photograph of a RF-heated rod may be seen in Fig. 5), air-steam mixture temperatures of 200°C and wall temperatures of 150°C to 200°C. In the first two tests, the air-steam mixture temperatures were 1000°C to simulate thermal equilibrium conditions in a tungsten target assembly. However, the gas temperatures did not cool to the surroundings temperature until entering the condenser, so the gas temperature was reduced in subsequent tests but still above the steam saturation temperature. Air-steam mixtures with steam mole fractions of 0.0, 0.07, 0.14, 0.30, 0.60, 0.80, 0.85 and 1.00 were tested. The test matrix for these tests is given in Table 2.

4.1 Tungsten Oxidation

It was observed that the tungsten oxidation rate was greatest in all air and least in all steam, varying non-linearly with increasing steam mole fraction as shown in Fig. 6. The normalized (dimensionless) tungsten oxidation rates for these experiments shown in Fig. 6 are defined as,

$$\dot{m}^*_{W,ox} = \dot{m}''_{W,ox} / \dot{m}''_{W,steam} \quad (3)$$

where $\dot{m}''_{W,ox}$ are the measured overall tungsten oxidation rates listed in Table 4 (column 3) and $\dot{m}''_{W,steam}$ are the tungsten vaporization rates for each experiment as calculated by Eq. (1) and listed in Table 4 (column 5) for the case of all steam. The data points shown in Fig. 6 are the averages of all the normalized tungsten oxidation rates for a given steam mole fraction. The tungsten oxidation rates in all air were more than five times greater than the tungsten oxidation rates in all steam as can be seen in Fig. 6. In all air, the tungsten which was oxidized remained on the rod as a growing scale of oxide with no downstream transport. In all steam, the tungsten which oxidized was immediately and completely vaporized by hydration and was transported downstream as a fine aerosol smoke as the tungstic-acid vapor condensed in the cold gas. For air-steam mixtures, most of the tungsten which was oxidized remained on the rods as a surface scale while some was vaporized and transported downstream. A post-test photograph of a tungsten rod from a test with a 0.6 steam mole fraction showing the oxide scale is shown in Fig. 7. The results of the gravimetric analyses for each test are listed in Table 3.

4.2 Tungsten Vaporization

The tungsten vaporization rate was zero in all air and varied with increasing steam mole fraction as shown in Fig. 8. The normalized (dimensionless) tungsten vaporization rates for these experiments shown in Fig. 8 are defined as,

$$\dot{m}^*_{W,vap} = \dot{m}''_{W,vap} / \dot{m}''_{W,steam} \quad (4)$$

where $\mathring{m}''_{W,vap}$ are the measured tungsten vaporization rates listed in Table 4 (column 4) and $\mathring{m}''_{W,steam}$ are the tungsten vaporization rates for each experiment as calculated by Eq. (1) and listed in Table 4 (column 5) for the case of all steam. The data points shown in Fig. 8 are the averages of all the normalized tungsten vaporization rates for a given steam mole fraction. The vaporization rates became maximum for steam mole fractions of approximately 0.85 and then decreased to the value predicted by Eq. (1) as the steam mole fraction approached unity (see Fig. 1 and [7]). It was only for steam mole fractions below 0.6 that the air limited the transport of steam to the surface. Above a steam mole fraction of 0.6, vaporization kinetics was the rate-limiting reaction; for steam mole fractions below 0.6, the vaporization rate fell off indicating that the vaporization rate was diffusion-limited and that increasing the fraction of air in the mixture increased the resistance to steam diffusion to the surface, thus decreasing the tungsten vaporization rate. The oxidation rate was never rate-limiting to vaporization; however the constantly decreasing oxidation rates with increasing steam mole fractions indicated that steam always presented a resistance to air diffusing to the surface.

4.3 Tungsten Aerosol Transport and Plateout

The tungsten-oxide which was transported downstream as condensation aerosols initially flowed upwards from the tungsten rods through an 18-inch long, one-inch diameter quartz tube, around a 3.5-inch radius, 90° bend and laterally through a 24-inch horizontal run. The entire length of the quartz glass flow path was heated by electrical resistance clamshell heaters which were individually controlled and measured. At the end of the quartz glass flow section, the tube made a 35° downward bend into the 12-inch long condenser which exited into the face of a 0.45

μm aerosol filter assembly. The tungsten-oxide plateout in the quartz tube was collected, nearly all of which was deposited near the exit into the condenser at the end of the heated zone which was cold. The tungsten-oxide which rained out in the condenser as the steam condensed was collected with the condensate and weighed after being dried. The aerosol smoke which escaped the condenser (see Fig. 9) was collected on the sub-micron filter assemblies which were then desiccated and reweighed to measure the aerosol burden.

For the case of all air, there was no aerosol transport so the plateout, condensate and smoke were all zero. For the case of all steam, there was very little plateout (several percent) and the rest of the aerosol was collected in the condensate from the condenser. There was no smoke discharge into the filters. For the experiments with intermediate air-steam fractions, there was aerosol plateout, aerosol in the condensate and aerosol smoke discharged from the condenser with the escaping air. The aerosol decontamination factors, DF, shown in Fig. 10 for these experiments are defined as,

$$DF = WO_{3,vaporized} / WO_{3,smoke} \quad (5)$$

where $WO_{3,vaporized}$ are the measurements of the total WO_3 generated by vaporization (Table 3, column 8) and $WO_{3,smoke}$ are the measurements of WO_3 aerosol discharged from the condenser and collected on the submicron filters (Table 3, column 6). The data points shown in Fig. 10 are the averages of all the DF's for a given steam mole fraction.

The normalized tungsten (or, equivalently, tungsten-oxide) aerosol discharge rates for these experiments shown in Fig. 11 are defined as,

$$\mathring{m}^*_{WO3,aerosol} = (0.793 \cdot \mathring{m}''_{WO3,aerosol}) / \mathring{m}''_{W,steam} \quad (6)$$

where $\mathring{m}''_{WO3,aerosol}$ are the measured tungsten-oxide aerosol discharge rates listed in Table 4 (column 6) and $\mathring{m}''_{W,steam}$ are the tungsten vaporization rates for each experiment as calculated by Eq. (1) and listed in Table 4 (column 5) for the case of all steam. The coefficient multiplier of 0.793 in the numerator of Eq. (5) is to convert the smoke discharge data from a measured mass of tungsten-oxide to the equivalent mass of tungsten-metal in order to properly normalize the equation by dividing by the calculated tungsten-metal vaporization rate. An equivalent methodology would be to multiply the denominator by 1.26 to convert the denominator into an equivalent mass of tungsten-oxide to represent the ratio of two masses of tungsten-oxide instead. The methodology shown in Eq. (6) was chosen because those variables are available in the numerical data in Table 4. The data points shown in Fig. 11 are the averages of all the normalized tungsten-oxide aerosol discharge rates at a single steam mole fraction.

4.4 Discussion

It has been found in these experiments that tungsten metal readily vaporizes in steam by chemical reactions with oxygen and steam in which tungsten-oxide is hydrated to tungstic acid vapor. The lower thermal limit for this reaction is between 700°C and 800°C. The oxidation of tungsten proceeds very effectively even in all air, however the vaporization of the oxide phase requires steam to support the hydration reaction. The aerosol generation rate increases with increasing steam mole fraction up to 0.85, then decreases thereafter as the steam mole fraction approaches unity. The normalized aerosol discharge rate defined in Eq. (6) exhibits a minimum

at both zero steam mole fraction and 100% steam mole fraction, indicating that there are competing effects which determine the magnitude of the aerosol release as a function of the steam mole fraction and which dominate at the asymptotes.

At low steam mole fractions, although the tungsten oxidation rates are high as shown in Fig. 6, the lack of steam retards the hydration reaction thus depressing the vaporization rates as shown in Fig. 8. At high steam mole fractions, although the tungsten oxidation rate is depressed due to the lack of free oxygen in the gas mixture as shown in Fig. 6, the abundance of steam enhances the hydration reaction thus enhancing the rates of tungsten vaporization as shown in Fig. 8. In fact, for the case of 100% steam, the vaporization reaction consumes all the oxide scale which forms on the exposed metal surface, leaving a fresh metal surface behind for continued oxidation and immediate vaporization. So although the oxidation rates are lower at high steam mole fractions, the vaporization reaction is more efficient and thus the vaporization rates are greater at high steam mole fraction.

The aerosol which was discharged in these experiments was first passed through a condenser to condense and remove the steam from the flowing gas mixture. This resulted in the removal of a portion of the aerosols along with the condensate. Therefore, the aerosol which was discharged from the exit of the condenser to be collected on the sub-micron aerosol filter assemblies was the result of both the aerosol generation rate and the aerosol removal processes downstream of the RF-heated zone, thus simulating the integral effects of passing the gas mixture through cold structures in which the steam would be condensed and retained. Although the tungsten vaporization rates at low steam mole fractions are small, the steam condensation effect is also small due to the small amount of steam present. So most of the aerosol which was

generated passed unaffected through the condensation region and was discharged onto the filter assemblies.; in other words, most of the little aerosol generated was discharged. Conversely, although the tungsten vaporization rates at high steam mole fractions are high, the steam condensation effect is also high due to the large fraction of steam present which is removed by condensation. So a smaller fraction of the aerosol which was generated was able to pass through the condensation region, most was rained out in the condenser by heterogenous condensation of steam on the aerosol particles themselves. In other words, only a little of the considerable aerosol generated was discharged.

Inspection of Fig. 11 reveals the dependence of the aerosol discharge rate upon the steam mole fraction which has just been discussed. The normalized aerosol discharge rates at the asymptotes, 0% and 100% steam mole fractions, tend toward zero for reasons of competing effects. At 0% steam mole fraction there is no vaporization to generate aerosols, so although there is no steam to condense there is no aerosol to discharge either. At 100% steam mole fraction there is considerable aerosol generation, however the condensers are 100% efficient at condensing the steam so that there is 100% retention of those aerosols in the condensate. What is interesting to note is that for steam mole fractions in the range of 5% to 90% steam mole fraction, the normalized aerosol discharge rates rapidly increase from zero to about 10% and remain between 10% to 30% over the entire range up to a steam mole fraction of approximately 90%. These measurements were difficult to make and there are numerous sources of potential error which are difficult to quantify. The authors recognize that there is an interesting structure to the dependence of the normalized aerosol discharge rates on the steam mole fractions within this range. However, the authors do not recommend placing a great deal of emphasis on these

trends, for instance the apparent minimum at a steam mole fraction of 0.60. Instead, at least until additional data are available, the authors conclude simply that for tungsten vaporization in air-steam mixtures of between 5% to 90% steam, the tungsten in the aerosol released as smoke from the experimentally-simulated condensation region is on the order of 10% to 30% of the tungsten vaporization rate predicted by Eq. (1). The data shown in Fig. 11 are listed in the tables, thus they are available for future analyses if such scrutiny is shown to be warranted. The clear result, however, is that in this intermediate region from 5% to 90% steam mole fraction, the competing effects of vaporization and condensation apparently compensate each other, resulting in an aerosol discharge rate which is essentially independent of the steam mole fraction within the specified bounds given above.

5. PRACTICAL SIGNIFICANCE

The use of tungsten in accelerator spallation targets is receiving continued and increasing consideration in accelerator applications as a result of its superior performance to most other high-Z solid materials in applications where maximum yields of neutrons or charged particles are desired. In addition, tungsten's favorable mechanical, thermal and thermodynamic properties facilitate the design, operation and maintenance of spallation targets in high-energy accelerator facilities, making installation, operation, target replacement and repair more routine than would be the case for a liquid-metal spallation target such as mercury or lead-bismuth eutectic.

As particle accelerators continue to evolve to higher energies and beam currents, the margins to the limits of the material properties of fixed targets will continue to decrease, rendering most other materials unsatisfactory for a number of reasons. Whereas tungsten can

survive to temperatures in excess of 3000 K, other metals and alloys such as platinum, Inconel and steel would fail at much lower temperatures. Although some accelerator applications may rule out the use of tungsten for reasons which may be fundamental, tungsten will continue to serve as a desirable spallation material, thus justifying continued research into its performance.

6. CONCLUSIONS

Earlier experiments with tungsten metal at high temperatures in all-steam [7, 8] demonstrated that the onset of tungsten vaporization would occur for temperatures in the 700-800 °C range and that the rate of vaporization obeyed an Arrhenius relationship of the form of Eq. (1). Since the gas in these experiments was all-steam, simply condensing the steam along a cold flow path effectively resulted in 100% retention of the tungsten-oxide aerosols which were formed. The experiments in the present paper were intended to investigate the oxidation and vaporization of tungsten and the removal of tungsten-oxide aerosols in air-steam mixtures to expand the data base to a more realistic and applicable range of operating conditions. The following observations and conclusions were made for the oxidation and vaporization of tungsten metal at 1000 °C in varying air-steam mixtures and the removal of tungsten-oxide aerosols in condensing systems.

1. The tungsten oxidation rate was observed to be maximum in all air and least in all steam. For air-steam mixtures between these two asymptotes, the oxidation rate achieved a plateau as shown in Fig. 6, first decreasing then increasing with increasing steam mole fraction, then dropping to a minimum at 100% steam.

2. The tungsten vaporization rate was observed to be greatest at a steam mole fraction of 0.85. As the steam mole fraction was increased to 100%, the tungsten vaporization rate then decreased monotonically to the value predicted by Eq. (1). As the steam mole fraction decreased to zero, the tungsten vaporization rate decreased monotonically to zero as well, the presence of steam being a necessary condition for tungsten-oxide to hydrate to the vapor phase.

3. The peak in the tungsten vaporization rate data at a steam mole fraction of 0.85 suggests that the free oxygen in air gave the optimal "boost" to the pre-oxidation reaction which is necessary for vaporization, while presenting the least resistance to diffusion of steam to the tungsten surface through the gas mixture; for steam mole fractions greater than 0.85, both oxidation and vaporization decreased, while for less steam the oxidation rate was minimally affected but the vaporization rate decreased to zero. In the one experiment in which air was replaced by argon, the tungsten vaporization rate was decreased to one-half the tungsten vaporization rate with air-steam while the tungsten oxidation rate was decreased by a factor of four, thus underscoring the enhancement effect of free oxygen on the reactions under consideration.

4. The retention of tungsten-oxide aerosols was investigated by collecting the aerosols from the discharge of the apparatus after the air-steam-aerosol mixture had passed through the condenser. Decontamination factors were high for the case of all steam and decreased rapidly as the air fraction was increased. The functional form of the data exhibited a somewhat non-linear trend at about 80% steam, then decreased monotonically to a value of unity at 100% air,

indicating that all of the aerosol generated would escape in the gas stream at a steam mole fraction close to zero. These data and the trends just described are shown in Fig. 10. However, these trends can be misleading because not only does the aerosol retention vary with the steam mole fraction, the tungsten vaporization rate varies as well. Therefore, Fig. 10 is actually the depiction of the ratio of two independent variables (aerosol formation and aerosol removal) which vary simultaneously with the steam mole fraction. The two effects cannot be separated in this presentation.

5. The data are presented in Fig.11 in a manner intended to demonstrate the integral effect of the air-steam mixture on the amount of aerosol released in the experiments from the exit of the condenser section as tungsten-oxide smoke. The mass of aerosol collected on the sub-micron filters is normalized by the vaporization rate given by Eq. (1) and presented as a function of the air-steam mixture. For the case of 100% steam, the fraction of Eq. (1) escaping in the smoke was zero because all the aerosol which was generated was washed out in the condensing steam. For the case of 100% air, the fraction of Eq.(1) escaping in the smoke went to zero because without steam (e.g., in all air) there was no vaporization and thus there was no smoke to release. For air-steam mixtures between these asymptotes in the range of 5% to 90% steam mole fraction, the fraction of Eq. (1) escaping in the smoke from the condenser rapidly increased from zero to about 10% and remained between 10% to 30% over the entire range. One would conclude, therefore, for tungsten vaporization in air-steam mixtures of between 5% to 90% steam, the tungsten in the aerosol released as smoke from the experimentally simulated condensation region is from 10% to 30% of the tungsten vaporization rate predicted by Eq. (1).

7. RECOMMENDATIONS AND FUTURE RESEARCH NEEDS

The rates of oxidation and vaporization of tungsten metal in air-steam mixtures have been investigated in this paper. Both rates are non-linear functions of the air-steam mixture, with the vaporization rate function peaking at a steam mole fraction of approximately 0.85 instead of 100% steam as was originally expected. This suggests that a little free oxygen in air gives the vaporization a "boost" by supporting the pre-oxidation reaction without the necessity of disassociating oxygen from steam. This "boost" is optimal at an air mole fraction of approximately 0.15. At greater air mole fractions, the air continues to "boost" the oxidation but appears to interfere with vaporization by limiting the diffusion of steam to the hot metal surface. A single experiment in which air was replaced by argon at (0.85 steam/0.15 argon) supports this conclusion; the 15%-argon depressed the vaporization rate by a factor of two and depressed the oxidation rate by a factor of approximately four below those for the case of 15%-air. It would be interesting to repeat the air-steam experiments with argon-steam mixtures as well as oxygen-steam mixtures over the same range of air mole fractions as in the present data to observe the trends in the oxidation and vaporization rates with argon and oxygen. Such tests would help to unravel the complex mass transfer and chemical kinetic effects which control the oxidation, vaporization and aerosol transport of tungsten metal at high temperatures.

REFERENCES

1. Miller, L. A., G. A. Greene and B. E. Boyack, "Accelerator Production of Tritium Programmatic Environmental Impact Statement Input Submittal," SAND 93-2094 (1996).

2. "Final Programmatic Environmental Impact Statement for Tritium Supply and Recycling," DOE/EIS-0161 (1995).

3. "Preliminary Safety Analysis Report," Accelerator Production of Tritium, PPO-POO-G-PSA-X-00001, Los Alamos National Laboratory (1998).

4. "APT Conceptual Design Report," Accelerator Production of Tritium, LA-UR-97-1329, Los Alamos National Laboratory (1997).

5. Unal, C., W. R. Bohl and K. Pasamehmetoglu, "Reaction of Tungsten in Steam Flow at High Temperatures," International Topical Meeting on Nuclear Reactor Thermal Hydraulics, NURETH-9, Paper No. 218, San Francisco, CA (1999).

6. Greene, G. A. and C. C. Finfrock, "Oxidation of Inconel 718 in Air at Temperatures From 973 K to 1620 K," Oxidation of Metals, 55(5/6), pp. 507-523 (2001).

7. Greene, G. A. and C. C. Finfrock, "Vaporization of Tungsten in Flowing Steam at High Temperatures," Int. J. Experimental Thermal and Fluid Science, 25, pp. 87-99 (2001).

8. Kilpatrick, M. and S. K. Lott, "Reaction of Flowing Steam With Refractory Metals III. Tungsten (1000°C -1700°C)," J. Electrochemical Soc., 113(1), pp. 17-18 (1966).

Table 1
Test Parameters and Experimental Measurements

Flow Geometry:	Initial flow direction vertically upwards from aerosol generator Vertical and horizontal flow segments, six-inch increments 90° bends in flow path, nominal 3.5 inch centerline radius of curvature One-piece quartz glass construction, one-inch diameter quartz glass
Wall Temperature:	Above the steam saturation temperature Wall temperature in range 150°C to 200°C Some tests with pre-set temperature gradients Inlet gas temperature set above the inlet wall temperature
Gas Mixture:	Argon gas during setup phase Air-steam mixture, preheated above wall temperature Steam mole fractions: 0.0, 0.07, 0.14, 0.30, 0.60, 0.80, 0.85 and 1.0 Gas temperature in range 200°C to 1000°C, pre-heated in packed bed
Tungsten Rod:	Pure tungsten rods used for aerosol source Rod diameter 3.0 mm, rod length 90 mm Rod temperature set to 1000°C RF heating of rod, temperature measured by optical pyrometer
Test Measurements:	Tungsten rod temperature, gas mixture inlet and flow path temperatures Tungsten mass loss Steam and air flow rates Tungsten-oxide mass distribution and overall tungsten-oxide collected

Table 2
Test Matrix of Temperatures and Flow Rates

Test	Steam Mole Fraction	T_W (°C)	T_{wall} (°C)	T_{gas} (°C)	M_{steam} (mole/min)	M_{air} (mole/min)
1S	0.60	996.0	200	1000	1.24E-01	8.43E-02
2S	0.58	997.5	197	1000	1.17E-01	8.43E-02
3S	0.54	997.1	199	177	1.01E-01	8.43E-02
4S	0.59	1000.7	209	185	1.21E-01	8.43E-02
5	0.59	1001.8	197	188	1.19E-01	8.43E-02
6	0.60	994.2	195	190	1.27E-01	8.43E-02
7	0.62	999.3	149	207	1.35E-01	8.43E-02
8	0.62	1004.9	164	209	1.35E-01	8.43E-02
9	0.00	1001.3	161	244	0.00	8.43E-02
11	0.00	1000.2	138	225	0.00	8.43E-02
10	1.00	1015.0	162	234	1.36E-01	0.00
12	1.00	1000.4	169	214	1.32E-01	0.00
13	0.32	1000.0	161	184	8.11E-02	1.69E-01
14	0.31	1000.1	148	195	7.50E-02	1.69E-01
15	0.80	985.2	150	225	1.03E-01	2.53E-02
16	0.81	998.6	154	237	1.08E-01	2.53E-02
17	0.07	999.2	154	203	1.36E-02	1.69E-01
18	0.14	1000.1	152	224	2.71E-02	1.69E-01
19	0.85	999.2	158	228	1.42E-01	2.53E-02
20	0.85	999.7	154	230	1.44E-01	2.53E-02
21	0.84	999.8	152	239	1.38E-01	2.54E-02
22*	0.84	1001.4	155	227	1.35E-01	2.54E-02

S Shakedown test, not used in analyses.
* Test 22 employed argon instead of air.

Table 3. Results of Gravimetric Analyses of Tungsten-Oxide Mass Distributions

Test	Steam Mole Fraction	Mass Distribution Analysis (g) ΔM_{rod} (M_f-M_i)	WO_3 in Condensate	WO_3 in Plateout	WO_3 in Smoke	WO_3 on Rod	WO_3 Vaporized	WO_3 Total	W-Metal Vaporized	W-Metal Oxidized
1S	0.60	0.029	0.287	0.000	0.023*	1.329	0.310	1.640	0.246	1.300
2S	0.58	-0.038	0.177	0.139	0.023*	1.113	0.339	1.452	0.269	1.151
3S	0.54	-0.078	0.322	0.059	0.030*	1.197	0.411	1.608	0.326	1.275
4S	0.59	-0.124	0.330	0.050	0.030*	0.969	0.409	1.378	0.325	1.093
5	0.59	-0.144	0.376	0.030	0.032	0.981	0.438	1.420	0.347	1.126
6	0.60	-0.153	0.273	0.040	0.028	0.569	0.341	0.909	0.270	0.721
7	0.60	-0.149	0.292	0.005	0.089	0.759	0.386	1.144	0.306	0.907
8	0.62	-0.122	0.359	0.033	0.042	1.070	0.434	1.504	0.344	1.192
9	0.00	0.550	0.000	0.000	0.000	2.656	0.000	2.656	0.000	2.106
11	0.00	0.430	0.000	0.000	0.000	2.076	0.000	2.076	0.000	1.647
10	1.00	-0.438	0.522	0.020	0.001	0.000	0.543	0.543	0.431	0.431
12	1.00	-0.248	0.302	0.007	0.010	0.000	0.319	0.319	0.253	0.253
13	0.32	-0.026	0.050	0.019	0.186	0.853	0.255	1.108	0.202	0.879
14	0.31	0.020	0.068	0.020	0.138	0.963	0.226	1.189	0.180	0.943
15	0.80	-0.083	0.189	0.018	0.023	0.478	0.230	0.708	0.182	0.562
16	0.81	-0.146	0.247	0.021	0.037	0.461	0.305	0.766	0.242	0.607
17	0.07	0.224	0.013	0.008	0.045	1.335	0.066	1.401	0.052	1.111
18	0.14	0.160	0.009	0.004	0.092	1.174	0.105	1.279	0.083	1.014
19	0.85	-0.092	0.210	0.018	0.007	0.457	0.235	0.692	0.186	0.548
20	0.85	-0.065	0.159	0.014	0.015	0.406	0.188	0.595	0.149	0.471
21	0.84	-0.083	0.185	0.021	0.003	0.401	0.209	0.610	0.166	0.484
22**	0.84	-0.119	0.130	0.002	0.025	0.024	0.157	0.181	0.124	0.144

S Shakedown test, not used in analyses. * Smoke discharge in Tests 1-4 are estimated from Tests 5-8. ** Test 22 employed argon instead of air.

Table 4
Tungsten Oxidation and Vaporization Rates and Tungsten-Oxide Aerosol Discharge Rates

Test	Steam Mole Fraction	Tungsten Reaction and Flow Rates ($g/cm^2 \cdot s$)			
		W Oxidation Rates	W Vaporization Rates		WO_3 Aerosol
		Measured	Measured	Calculated	Discharge Rates
1S	0.60	4.03E-05	9.94E-06	9.87E-06	-
2S	0.58	4.65E-05	1.08E-05	1.01E-05	-
3S	0.54	3.95E-05	1.01E-05	1.00E-05	-
4S	0.59	3.38E-05	1.00E-05	1.06E-05	-
5	0.59	3.32E-05	1.03E-05	1.08E-05	9.41E-07
6	0.60	2.31E-05	8.64E-06	9.60E-06	9.02E-07
7	0.62	2.82E-05	9.52E-06	1.04E-05	2.76E-06
8	0.62	3.77E-05	1.09E-05	1.13E-05	1.34E-06
9	0.00	6.64E-05	0.00	1.07E-05	0.00
11	0.00	5.19E-05	0.00	1.05E-05	0.00
10	1.00	1.36E-05	1.36E-05	1.31E-05	3.15E-08
12	1.00	9.52E-06	9.52E-06	1.06E-05	3.88E-07
13	0.32	2.73E-05	6.29E-06	1.05E-05	5.77E-06
14	0.31	2.75E-05	5.24E-06	1.05E-05	4.04E-06
15	0.80	3.53E-05	1.14E-05	8.36E-06	1.43E-06
16	0.81	3.83E-05	1.52E-05	1.03E-05	2.32E-06
17	0.07	4.55E-05	2.14E-06	1.04E-05	1.82E-06
18	0.14	4.32E-05	3.54E-06	1.05E-05	3.93E-06
19	0.85	4.20E-05	1.43E-05	1.04E-05	5.06E-07
20	0.85	4.60E-05	1.46E-05	1.04E-05	1.46E-06
21	0.84	3.66E-05	1.26E-05	1.05E-05	2.50E-07
22*	0.84	9.18E-06	7.95E-06	1.07E-05	1.59E-06

S Shakedown test, not used in analyses.
* Test 22 employed argon instead of air.

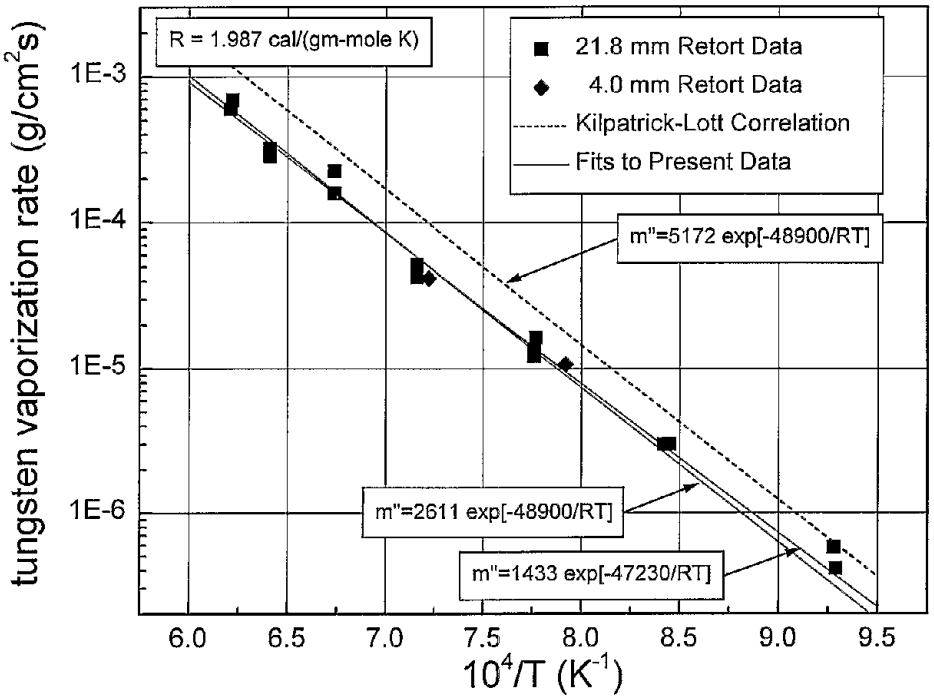

Figure 1. Tungsten-Metal Vaporization Rates in 100% Steam vs. Temperature [7]

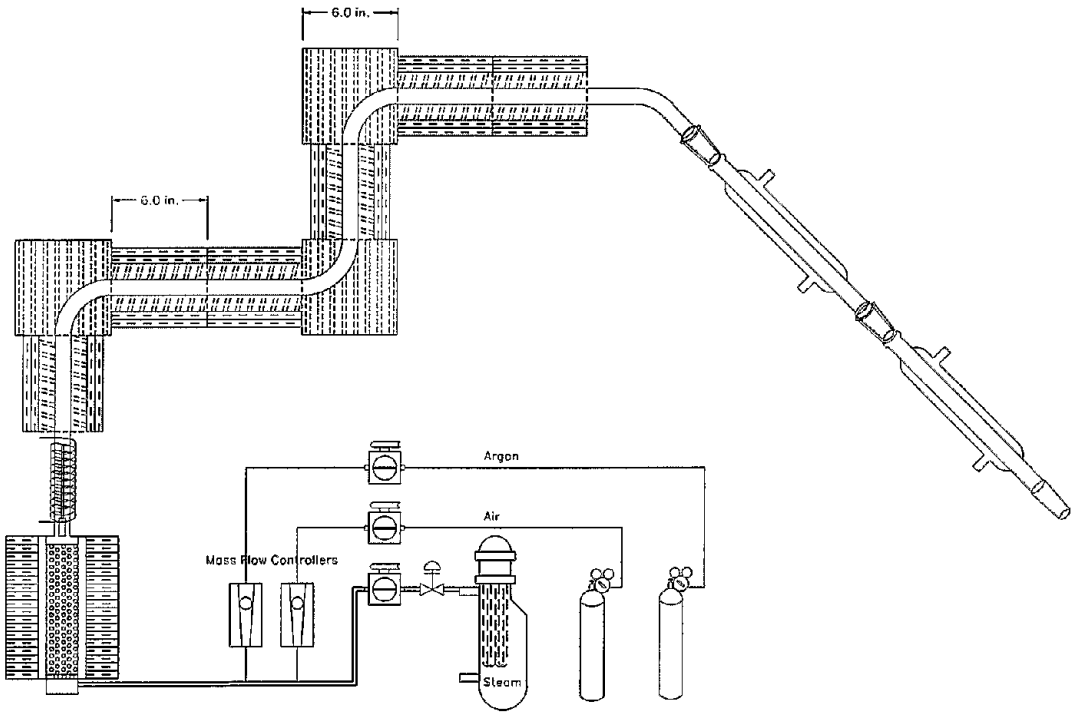

Figure 2. Schematic of the Aerosol Generation and Deposition Apparatus

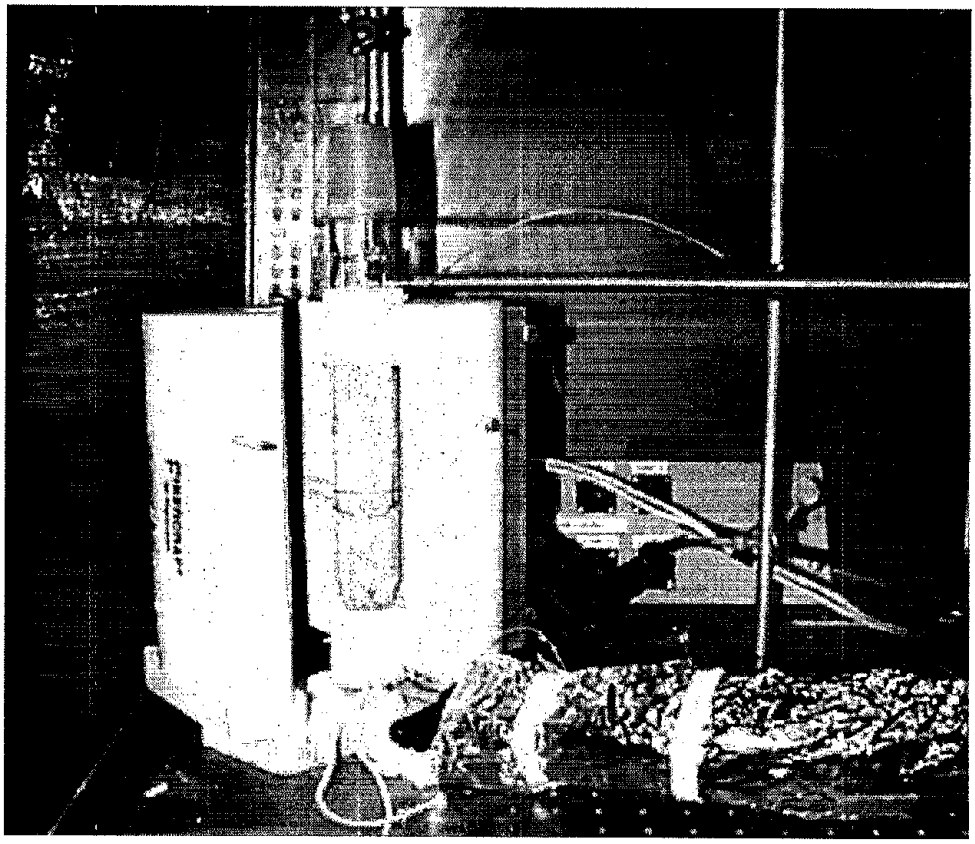

Figure 3. Photograph of Split Open Gas Mixture Heater Assembly

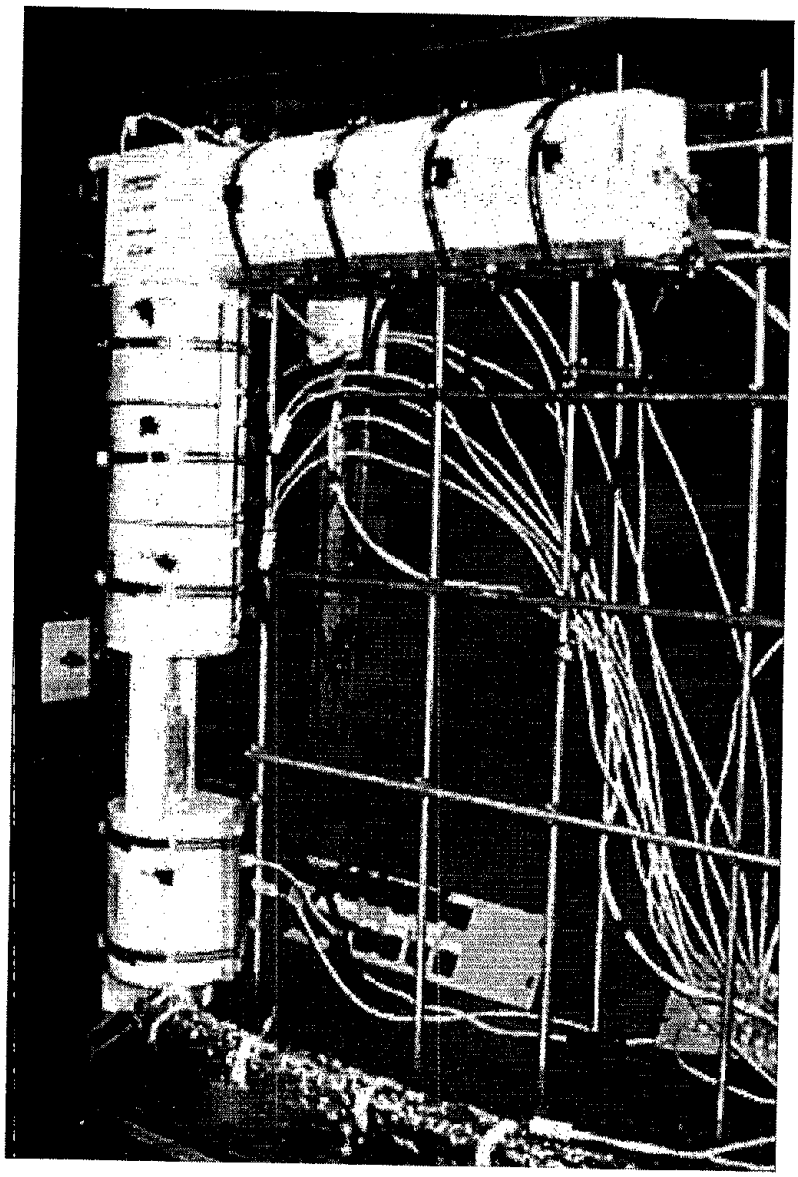

Figure 4. Photograph of Aerosol Generation, Transport and Deposition Apparatus

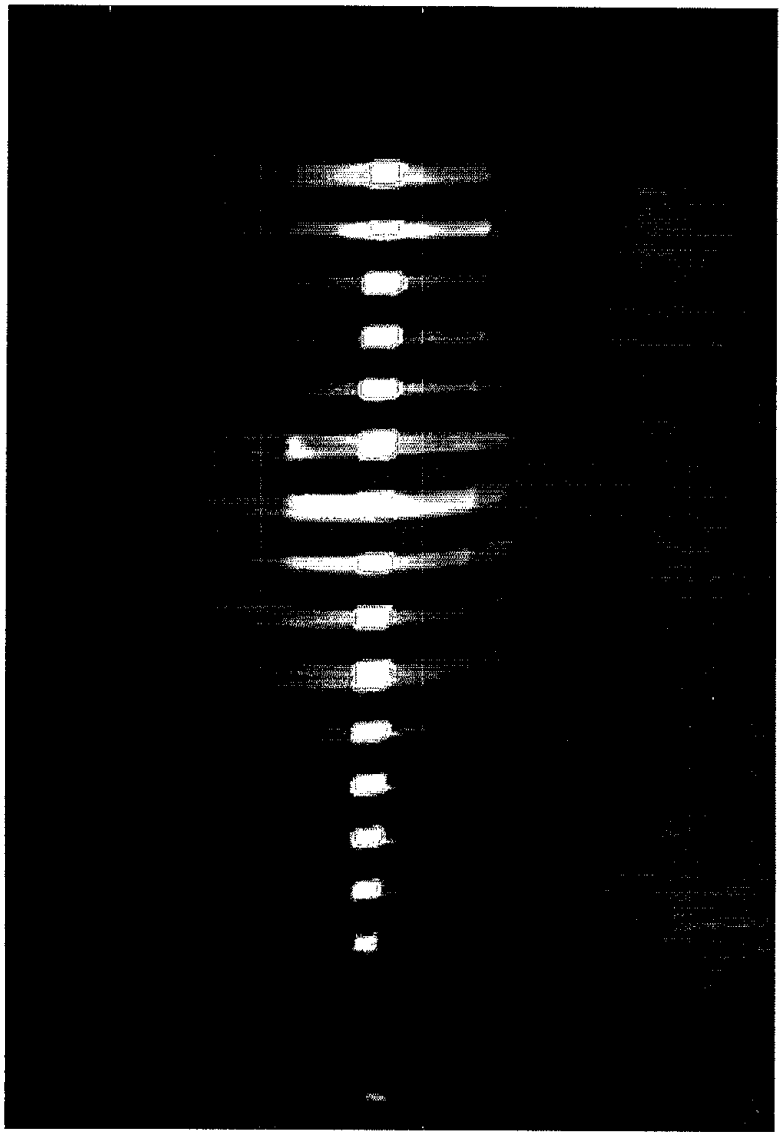

Figure 5. Photograph of RF-Heated Tungsten Rod at 1000°C

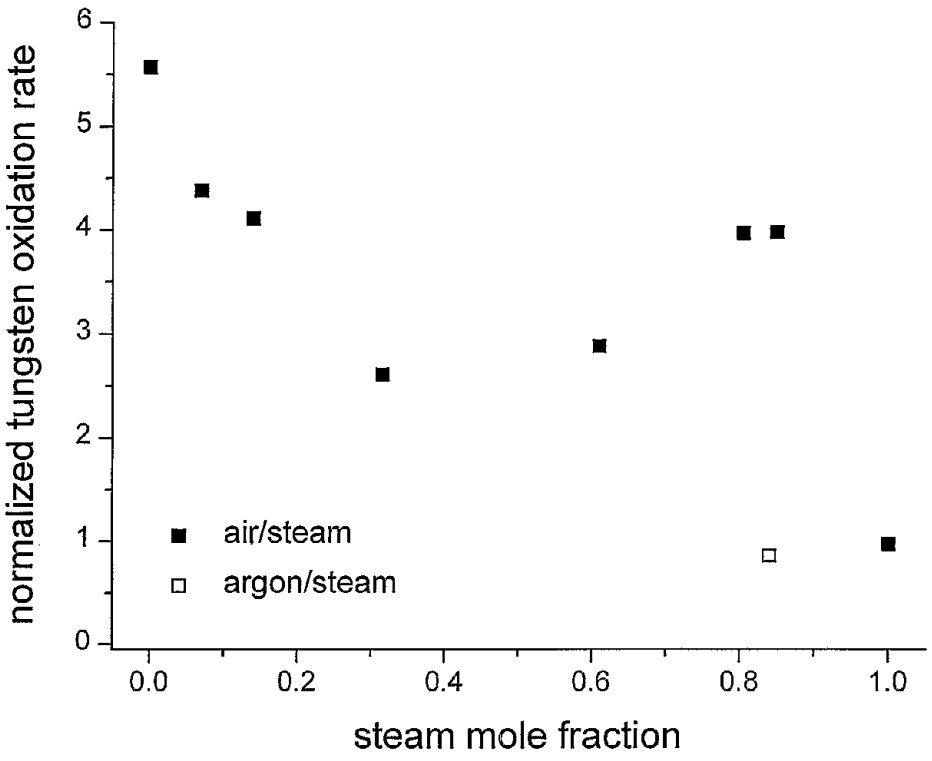

Figure 6. Normalized Tungsten Oxidation Rate vs. Steam Mole Fraction

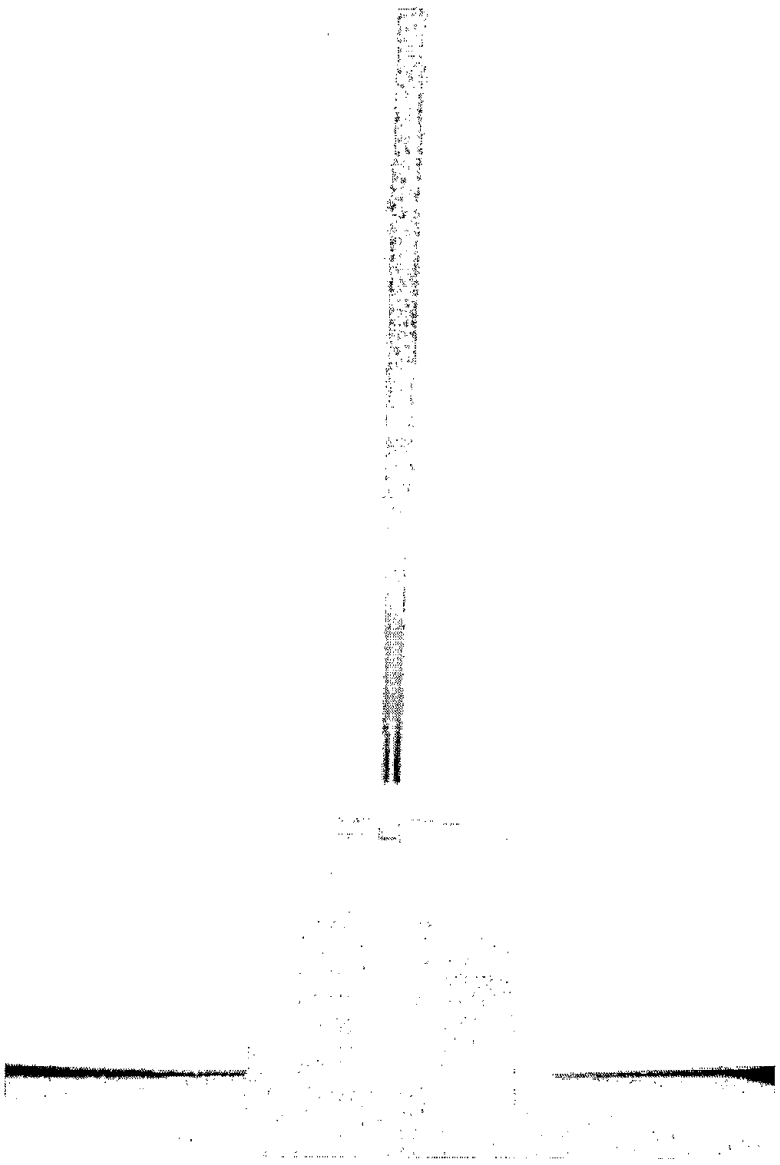

Figure 7. Photograph of Oxidized Tungsten Rod After Test

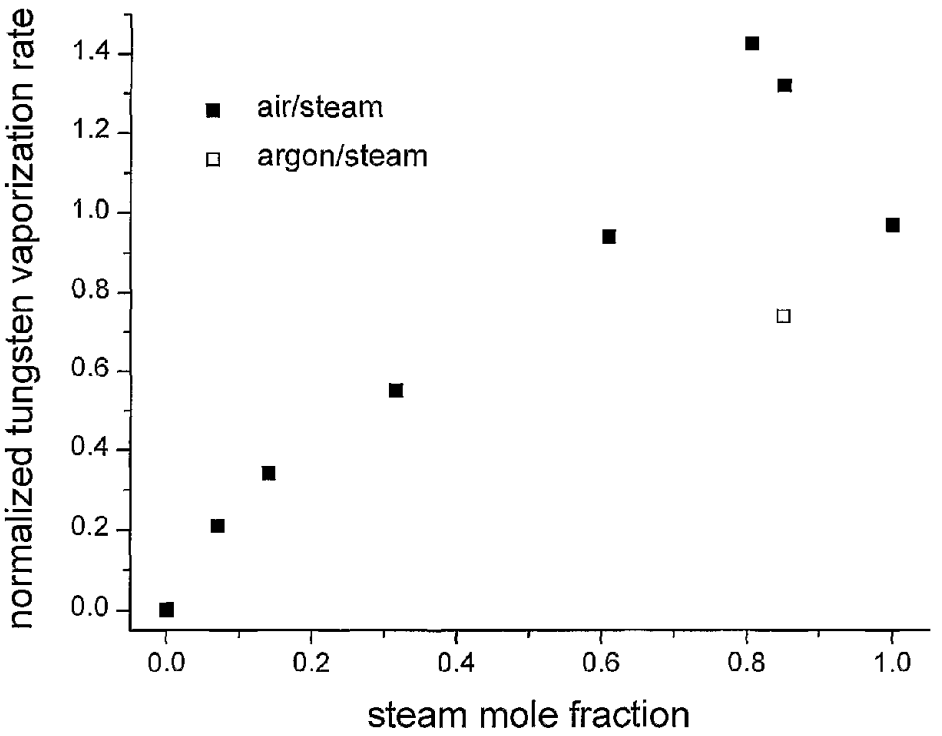

Figure 8. Normalized Tungsten Vaporization Rate vs. Steam Mole Fraction

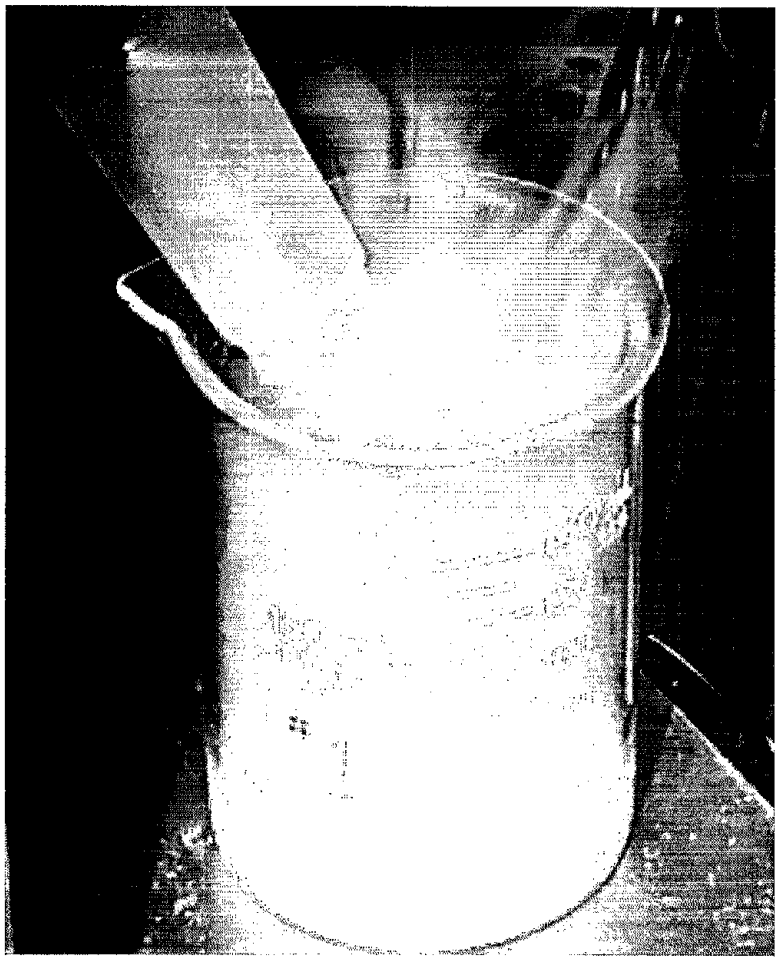

Figure 9. Photograph of Tungsten-Oxide Aerosol Exiting the Condenser

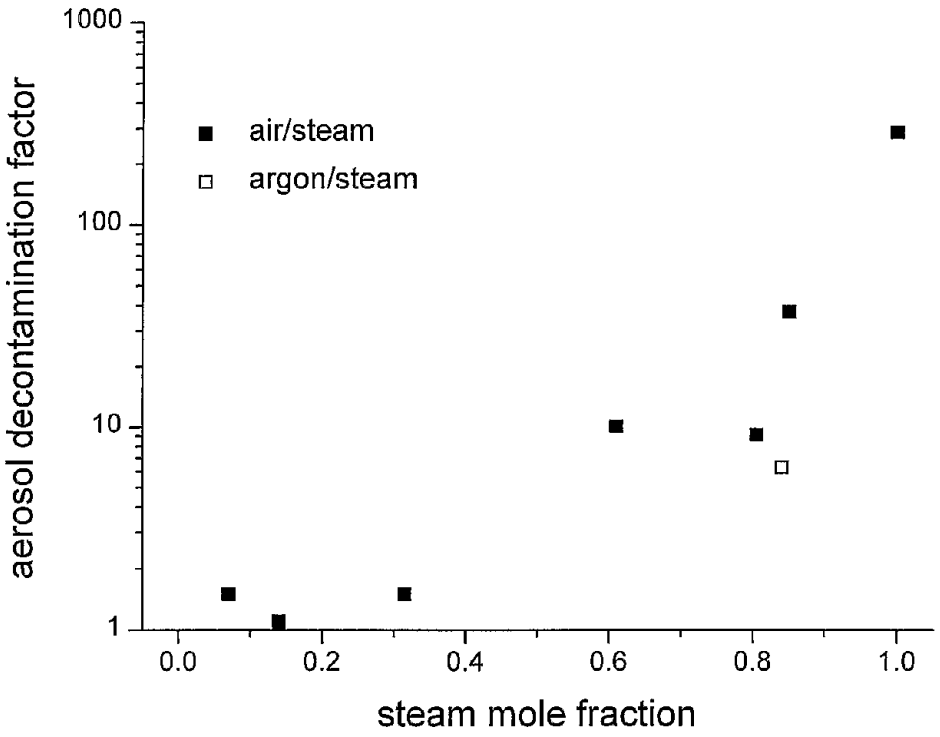

Figure 10. Tungsten-Oxide Aerosol Decontamination Factor vs. Steam Mole Fraction

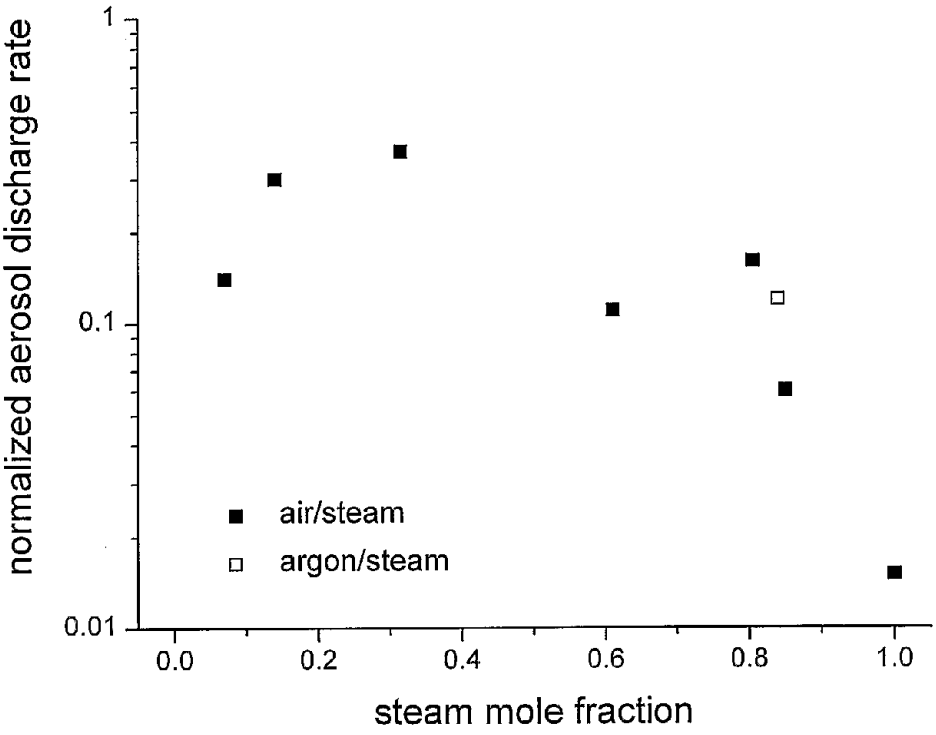

Figure 11. Normalized Tungsten-Oxide Aerosol Discharge Rate vs. Steam Mole Fraction